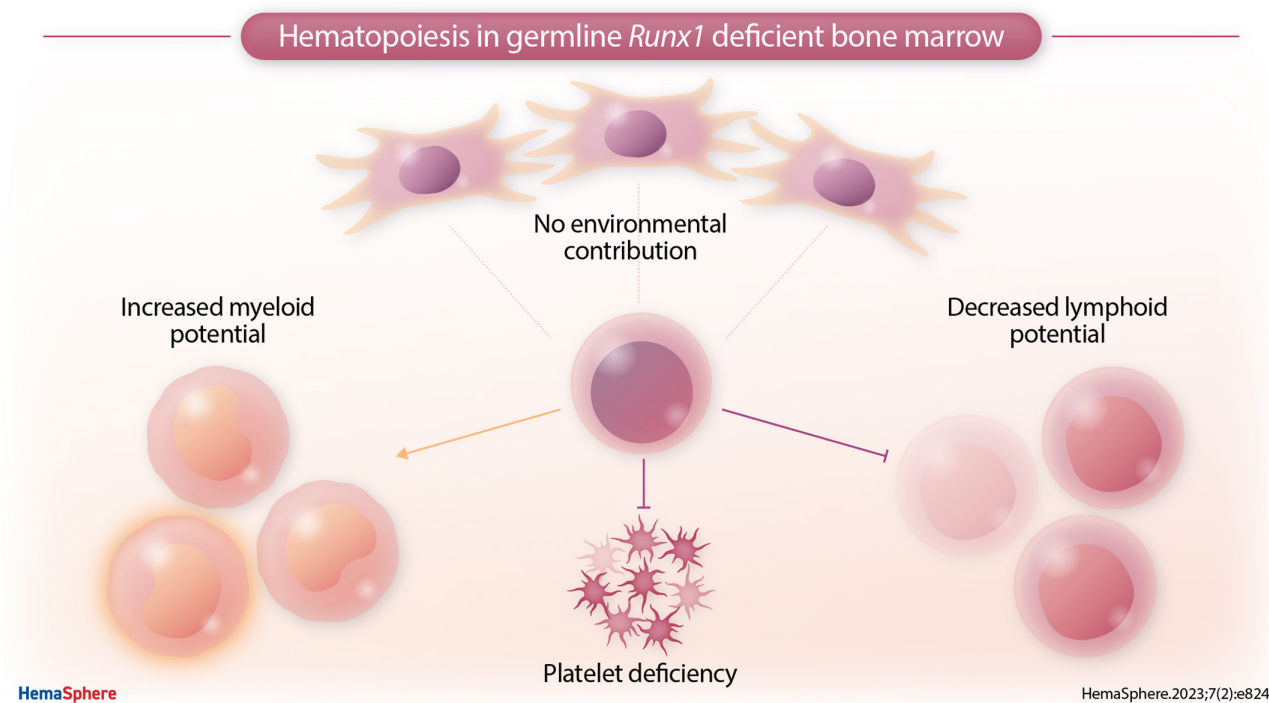# Hematopoietic Cell Autonomous Disruption of Hematopoiesis in a Germline Loss-of-function Mouse Model of *RUNX1*-FPD

Martijn P. T. Ernst[1], Eline Pronk[1], Claire van Dijk[1], Paulina M. H. van Strien[1], Tim V. D. van Tienhoven[1], Michiel J. W. Wevers[1], Mathijs A. Sanders[1], Eric M. J. Bindels[1], Nancy A. Speck[2], Marc H. G. P. Raaijmakers[1]

Hematopoiesis in germline *Runx1* deficient bone marrow

No environmental contribution

Increased myeloid potential

Decreased lymphoid potential

Platelet deficiency

HemaSphere

Hematopoietic Cell Autonomous Disruption of Hematopoiesis in a Germline Loss-of-function Mouse Model of *RUNX1*-FPD

Martijn P. T. Ernst[1], Eline Pronk[1], Claire van Dijk[1], Paulina M. H. van Strien[1], Tim V. D. van Tienhoven[1], Michiel J. W. Wevers[1], Mathijs A. Sanders[1], Eric M. J. Bindels[1], Nancy A. Speck[2], Marc H. G. P. Raaijmakers[1]

Correspondence: Marc H. G. P. Raaijmakers, (m.h.g.raaijmakers@erasmusmc.nl).

ABSTRACT

RUNX1 familial platelet disorder (*RUNX1*-FPD) is a hematopoietic disorder caused by germline loss-of-function mutations in the *RUNX1* gene and characterized by thrombocytopathy, thrombocytopenia, and an increased risk of developing hematologic malignancies, mostly of myeloid origin. Disease pathophysiology has remained incompletely understood, in part because of a shortage of *in vivo* models recapitulating the germline *RUNX1* loss of function found in humans, precluding the study of potential contributions of non-hematopoietic cells to disease pathogenesis. Here, we studied mice harboring a germline hypomorphic mutation of one *Runx1* allele with a loss-of-function mutation in the other *Runx1* allele (*Runx1$^{L148A/-}$* mice), which display many hematologic characteristics found in human *RUNX1*-FPD patients. *Runx1$^{L148A/-}$* mice displayed robust and pronounced thrombocytopenia and myeloid-biased hematopoiesis, associated with an HSC intrinsic reconstitution defect in lymphopoiesis and expansion of myeloid progenitor cell pools. We demonstrate that specific deletion of *Runx1* from bone marrow stromal cells in *Prrx1-cre;Runx1$^{fl/fl}$* mice did not recapitulate these abnormalities, indicating that the hematopoietic abnormalities are intrinsic to the hematopoietic lineage, and arguing against a driving role of the bone marrow microenvironment. In conclusion, we report a *RUNX1*-FPD mouse model faithfully recapitulating key characteristics of human disease. Findings do not support a driving role of ancillary, non-hematopoietic cells in the disruption of hematopoiesis under homeostatic conditions.

INTRODUCTION

RUNX1 familial platelet disorder (*RUNX1*-FPD) is a rare disease caused by germline variants in the *RUNX1* gene, including missense, nonsense, and splice-site single nucleotide variants. Most affected families harbor a unique mutation.[1] The clinical phenotype of *RUNX1*-FPD consists of a bleeding diathesis due to quantitative and qualitative platelet defects and a propensity to develop myeloid and lymphoid hematologic malignancies that can present at any age.[1,2] Patients are particularly at risk to develop acute myeloid leukemia (AML) and myelodysplastic syndrome,[1,2] with an estimated lifetime risk of about 44%.[3] Other hematological malignancies have also been described in these patients, of which T-cell acute lymphoblastic lymphoma is the most common.[1] The biological mechanisms through which monoallelic germline *RUNX1* mutations drive the hematologic defects and malignant transformation remain incompletely understood. Additionally, it is unclear whether these mechanisms are identical among different *RUNX1* mutations. Functional investigation of some *RUNX1* variants indicated that mutations might confer a dominant-negative effect, while others result simply in a non-functional allele.[4–6] It has been suggested that dominant-negative mutations might confer a higher propensity to develop malignancy than loss-of-function mutations.[4,6,7]

Runx1 knockout in mice is embryonic lethal, precluding the analysis of germline loss-of-function effects on hematopoiesis.[8,9] To circumvent this limitation, existing models have focused on the targeted deletion of *Runx1* from the hematopoietic lineage,[10–18] precluding the analysis of the potential effect of *Runx1*-deficient non-hematopoietic cells on disease phenotypes, or germline deletion of *Runx1* in a heterozygous manner (*Runx1$^{+/-}$* mice),[19] likely not fully recapitulating dominant-negative effects of a subset of mutations in human disease. None of the existing mouse models have documented myeloid transformation in the absence of experimentally induced secondary mutations, leading to the notion that *Runx1* deficiency in hematopoietic cells is not sufficient to drive neoplastic alterations.

Genetically altered non-hematopoietic cells may, however, contribute to the disruption of hematopoiesis (including bone marrow failure) and myeloid transformation. In particular, bone

marrow mesenchymal stromal cells (BMSCs) form a major constituent of the bone marrow niche and have a key role in hematopoietic stem and progenitor cells (HSPCs) regulation.[20,21] Primary genetic alterations in these cells were able to drive hematopoietic disruption and malignant transformation in mice,[22–24] with mechanistic implications of NF-kB-associated inflammatory activation of BMSCs inducing genotoxic stress in HSPCs.[25]

Runx1 is expressed in cells of the mesenchymal lineage, contributing to bone formation and homeostasis,[26–28] and its deficiency has been linked to inflammatory activation of diverse cell types, including alveolar epithelial cells,[29] HSPCs[30] and neutrophils,[31] warranting studies addressing potential contributions of *RUNX1* deficiency in BMSCs to hematopoietic phenotype and in particular malignant transformation in *RUNX1*-FPD.

Here, we report the hematopoietic characterization of a *RUNX1*-FPD mouse model induced by a hypomorphic mutation in the Runt homology domain on a null background, mimicking the germline nature of decreased residual *RUNX1* function caused by dominant-negative mutations, which are suggested to constitute a subset of missense mutations found in *RUNX1*-FPD patients.[4,5] This model faithfully recapitulates key hematopoietic characteristics of human disease. Contributions of the bone marrow environment to the hematopoietic phenotype are addressed by transplantation studies complemented by the generation of mouse models with targeted deletion of *Runx1* from BMSCs. Collectively, findings support a model of hematopoietic cell-intrinsic disruption of hematopoiesis in *RUNX1*-FPD, without major contributions of the bone marrow microenvironment to the hematopoietic phenotype under homeostatic conditions.

MATERIALS AND METHODS

Mice

Runx1[L148A/+] (Runx1[tm9Spe])[32] and *Runx1*^{fl/+} (*Runx1*[tm3.1Spe])[11] have been reported before. Cryopreserved *Runx1*^{+/−} (*Runx1*[tm1Dow])[8] mouse spermatocytes were present in the Experimental Animal Center (EDC) of the Erasmus MC. *Prx1-cre (Tg(Prrx1-cre)1Cjt)*[33] and Rosa26-tdTomato (B6.Cg-Gt(ROSA)26Sortm9(CAG-tdTomato)Hze/J)[34] mice were purchased from The Jackson Laboratory. *Ptprc^a Pepc^b/BoyCrl* (B6.SJL) mice were purchased from Charles River. The mice were housed in individually ventilated cages under specific pathogen-free conditions in the Erasmus MC EDC, according to institutional guidelines. Water and food were provided *ad libitum*. All mouse experiments were approved by the Animal Welfare/Ethics Committee of the EDC in accordance with legislation in the Netherlands (approval No. EMC 2067, 2714, 2892, 3062).

Tissue collection

Mice were weighed, and peripheral blood was obtained via submandibular vein puncture. Blood was collected in K2EDTA-coated microtainers, and automated blood count analysis was performed using a Scil Vet abc Plus+ counter (HORIBA Medical, Kyota, Japan). The mice were euthanized by cervical dislocation, and single-cell suspensions of bone marrow and bone fraction were prepared from the hind legs of mice as previously described.[22] In brief, hind legs were stripped from soft tissue, and bones were crushed and washed in PBS (Gibco) with 0.5% FCS. Cell suspensions were mechanically dispersed through a 40-µm nylon mesh cell strainer (Corning) and pelleted at 600*g*, followed by lysis of red blood cells using ACK lysis buffer (Lonza). Cells were subsequently washed and filtered using a 40-µm strainer. To determine bone marrow cellularity, single-cell suspensions, derived from 1 femur, were mixed 1:1 with Trypan Blue (Invitrogen), and the viable cell count was determined using a Countess 3 Cell Counter (Invitrogen). Remnants of crushed bones (bone fraction) were incubated with collagenase for 45 minutes at 37°C, washed with PBS, and filtered through a 40µm strainer. The remaining red blood cells in bone fraction were lysed using ACK lysis buffer (Lonza) and washed again with PBS, followed by another filtration through a 40-µm cell strainer.

Genotyping

Genomic DNA was extracted from tissues using lysis buffer containing 10% SDS solution (Lonza AccuGENE), 1M Tris pH 8.5 (Merck), 0.5M EDTA (Lonza), 5M NaCl, Proteinase K (Roche), and TE-buffer (VWR Life Sciences). After lysis, the extracted DNA was dissolved in TE buffer (VWR Life Sciences). Blood and bone marrow cells were pelleted before lysis at room temperature and 4°C, respectively, by centrifugation at 600*g*. Polymerase chain reaction (PCR), using the primers listed below, and subsequent gel electrophoresis were performed to verify genotype and Cre-mediated recombination in genomic DNA samples.

Primer set sequences	Allele/band size basepairs
Fw: GAGTCCCAGCTGTCAATTCC	Runx1 +/ 400
Rv: GGCAAC TTGTGGCGGATTTG	Runx1 L148A/ 450
Fw: GCCATCACAGTGACCAGAGTGC	Runx1 +/ 400
Rv(1): CTGTACCAATGAGAAACAGTAGTAGC	Runx1 −/ 600
Rv(2): CGGCAGGCCCTGCCATAGC	
Fw: CCCACTGTGTGCATTCCAGATTGG	Runx1 +/ 200
Rv(1): GACGGTGATGGTCAGAGTGAAGC	Runx fl/ 275
Rv(2): CACCATAGCTTCTGGGTGCAG	Runx del/ 310
Cre Fw: GCGGTCTGGCAGTAAAAACTATC	Prrx1-cre +/100
Cre Rv: GTGAAACAGCATTGCTGTCACTT	Control/324
Ctrl Fw: CTAGGCCACAGAATTGAAAGATCT	
Ctrl Rv: GTAGGTGGAAATTCTAGCATCATC	

Hematopoietic stem cell transplantation

Recipient mice were lethally irradiated (single dose of 8.5 Gy) at ages 8–16 weeks and transplanted within 24 hours after irradiation. Fresh single-cell suspensions of viable bone marrow cells were prepared as described above and filtered through a 40-µm FACS tube strainer (Falcon) shortly before injection. Mice were transplanted with 1×10^6 viable fresh bone marrow cells in 200 µL PBS for transplant-in studies and 0.75×10^6 viable thawed cryopreserved bone marrow cells in 200 µL PBS for transplant-out studies. For competitive transplants, fresh viable SJL bone marrow cells (age 12 weeks) were mixed with viable *Runx1*^{+/+} or *Runx1*[L148A/−] bone marrow cells (age 7 months) (1:1 ratio) after counting viable cells as previously described. Single-cell suspensions were injected intravenously in the tail vein of recipient mice. Mice received antibiotic-supplemented (Baytril) autoclaved water for 3 subsequent weeks after transplantation.

Flow cytometry and flow cytometry-assisted cell sorting

To identify HSPC subsets, single-cell suspensions of bone marrow were stained by incubating for 20 minutes at 4°C with fluorescently labeled antibodies directed against murine cell surface markers: eFluor450 anti-CD34 (eBioscience Catalog # 48-0341-82), Pacific Blue anti-Sca1 (Biolegend Catalog #108120), PE-Texas Red anti-cKit (BD Biosciences Catalog #562417), APC-Cyanine7 anti-CD16/CD32 (BD Biosciences Catalog #560541), APC anti-FLT3 (eBioscience Catalog #17-1351-80). Additionally, cell suspensions were simultaneously stained with a lineage cocktail consisting of the following biotinylated antibodies: anti-B220 (BD Biosciences Catalog # 553086), anti-Mac1 (BD Biosciences Catalog #553309), anti-Ter119 (BD Biosciences Catalog #553672), anti-CD8a (BD Biosciences Catalog #553029), anti-CD3e (BD Biosciences Catalog #553060), anti-CD4 (BD Biosciences Catalog #553728), anti-Gr1 (BD Biosciences Catalog #553125). In

transplantation experiments, donor and recipient cells (or test and competitor cells) were distinguished by staining with FITC anti-CD45.1 (Biolegend Catalog#110706) and either APC anti-CD45.2 (ThermoFisher Catalog#17-0454-82), APC-Cyanine7 anti-CD45.2 (Biolegend Catalog#109824) or Pe-Cyanine7 CD45.2 (Biolegend Catalog#109829). After incubation, cells were washed with FACS buffer and centrifuged for 5 minutes at 600xg at 4°C. Cell pellets were resuspended in Pacific Orange-Streptavidin (ThermoFisher Scientific Catalog # S32365) and incubated for 10 minutes at 4°C. After washing, cells were further stained for viability using 7AAD (Beckman Coulter, Catalog #B88526), and data were acquired using a BD FACSAria III or a BD FACSymphony A5 and BD FACSDiva software (BD bioscience).

To identify differentiated hematopoietic cells in blood and bone marrow samples, single-cell suspensions were stained as previously described for cell surface markers using the following fluorescently labeled antibodies directed against murine cell markers: Alexa Fluor 700 anti-Gr1 (Biolegend Catalog #108422), PE-Cyanine7 anti-Mac1 (Biolegend Catalog #101215), Pacific Blue anti-B220 (eBioscience Catalog #15-0452-83), PE anti-CD45.1 (Biolegend Catalog #110709), BV510 anti-CD3e (Biolegend Catalog #563024), and APC-Cyanine7 anti-CD45.2 (Biolegend Catalog # 109824). Stainings were performed as mentioned before, and samples were analyzed using a BD LSR II Flow Cytometer or BD FACSymphony A5.

To isolate stromal subsets, bone fraction samples were stained for extracellular markers with the following fluorescently labeled antibodies: APC-Cyanine7 anti-CD45.2 (Biolegend Catalog #109824), APC-Cyanine7 anti-CD45.1 (Biolegend Catalog #110716), BV510 anti-Ter119 (Biolegend Catalog #116237), APC-R700 anti-CD31 (BD Biosciences #565509), PE anti-CD51 (Biolegend Catalog #104105), Pacific Blue anti-Sca1 (Biolegend Catalog #104105), APC anti-CD140a (eBioscience Catalog #17-1401-81). Stainings were performed as described above, and cells were sorted into 800 μL TRIzol (ThermoFisher Scientific Catalog #15596018) using a BD FACSAria III or analyzed using a BD FACSymphony A5. To define deletion efficiency in stromal subsets, the aforementioned procedure was performed with the addition of biotinylated anti-CD51 (Biolegend Catalog#104103), biotinylated anti-LepR (Bio-Techne Catalog#BAF497), Streptavidin BV785 (Biolegend Catalog#405249) and Zombie NIR (Biolegend Catalog#423105).

RNA sequencing

RNA isolation, cDNA preparation, and library preparation were performed as previously described.[35–37] Briefly, RNA was extracted from sorted cell populations using the standard protocol of RNA isolation with TRIzol and GenElute LPA (Sigma). cDNA was generated using a SMARTer Ultra Low RNA Kit (Clonetech) for Illumina Sequencing following the manufacturer's guidelines. Amplified cDNA was processed according to the TruSeq Sample Preparation v.2 Guide (Illumina) and paired end-sequenced (2 × 101 bp) on the NovaSeq 6000 (Illumina). Samples were demultiplexed using bcl2fastq (v2.20; Illumina), after which fastqc (v0.11.9[38]) was used to generate quality metrics for the generated FASTQ files. SMARTer sequencing adapters were trimmed from the reads using fqtrim (v0.9.7[39]). Reads were pseudo-aligned against the mouse reference genome mm10 (Ensembl build 104) using Salmon (v1.4[40]) to generate transcript quantification files. These transcript quantification files were used as input for tximport (v1.24.0[41]) in combination with DESeq2 (v1.30.1[42]) to perform differential expression analysis within R (v4.0.2). Subsequently, genes were ranked according to their Adaptive SHRunken (v2.2-54[43]) log2 foldchange and stored in rank files. The rank files were then used as input for pre-ranked Gene-Set Enrichment Analysis (GSEA;

v3.0[44,45]) utilizing gene sets from MsigDB (v7.2[45,46]) gene-set libraries C2, C5, and Hallmark. Pre-ranked GSEA was performed using 1e4 gene-set permutations and the classic enrichment score scheme.

In addition, the DEXSeq (1.42.0[47,48]) R package was used separately to find differential exon expression of the *Runx1* gene.

Data analysis

Flow cytometry data were analyzed using FlowJo software (version 10.8.1, Treestar). *P* values were calculated using statistical tests as stated in the figure legends using IBM SPSS software (version 28.0.1.0). Statistical significance was tested via ANOVA and the Tukey-Kramer HSD post-hoc test in the case of 3 experimental groups and the Student's t-test in the case of 2 experimental groups. P-values of less than 0.05 were considered significant, which is indicated in the figures by asterisks (*$P <$ 0.05, **$P <$ 0.01, ***$P <$ 0.001). Graphs were generated using GraphPad Prism (version 9.3.1).

RESULTS

Mice with germline *Runx1* deficiency leading to less than 50% residual RUNX1 function

Human *RUNX1*-FPD is genetically characterized by congenital monoallelic *RUNX1* mutations. Mutations associated with *RUNX1*-FPD can create non-functional or dominant-negative alleles,[4–7] with missense mutations mainly clustering in the RUNT homology domain (RHD).[1,49] To study the gene dose effects of *Runx1* deficiency and the *in vivo* consequences of a residual RUNX1 function below 50%, as might be caused by dominant-negative mutations, we crossed *Runx1^L148A/+* mice,[5,32,50] harboring a hypomorphic point mutation in the RHD (Figure 1A) with *Runx1^+/-* mice,[8] generated via an insert that disrupts the RHD by introducing premature stop codons in all reading frames (Figure 1A). Interbreeding these mouse strains resulted in *Runx1^+/+* (wild type), *Runx1^L148A/+*, *Runx1^+/-* and *Runx1^L148A/-* mice. Mice were born in Mendelian frequencies, but a subset of *Runx1^L148A/-* mice (36%) displayed early postnatal lethality and were eaten by their mother, precluding in depth analysis. Surviving *Runx1^L148A/-* mice were runted, which persisted upon aging with a significantly lower body weight in 7–8-month-old *Runx1^L148A/-* mice compared to controls (Suppl. Figure S1).

Runx1^L148A/- mice display thrombocytopenia and a defect in lymphopoiesis

Runx1^L148A/- mice displayed thrombocytopenia—an important feature of *RUNX1*-FPD—with robustly and significantly decreased platelet numbers in comparison to both wild type and *Runx1^L148A/+* animals (Figure 1B). No significant differences were found in the leukocyte numbers and hemoglobin levels, but immunophenotypic analyses revealed a non-significant increase in (Gr1+Mac1+) granulocytes and reduction in (B220+) B-cell numbers in *Runx1^L148A/-* mice (Figure 1B, C; Suppl. Figure S2A), with a resulting increase in the granulocyte to lymphocyte ratio, indicative of myeloid skewing in the peripheral blood (Figure 1C).

Cellularity of the bone marrow was unaltered in *Runx1^L148A/-* mice compared to controls (Figure 1D), but there was a significant reduction of B-cell numbers in *Runx1^L148A/-* mice in comparison to *Runx1^L148A/+* mice with a resulting increase of the myeloid/lymphoid ratio, reflecting findings in the peripheral blood (Figure 1E; Suppl. Figure S2B).

The number of immunophenotypic long-term (LT) (lin⁻cKit+Sca1+ (LKS) CD34⁻Flt3⁻) hematopoietic stem cells (HSCs) was unaltered in *Runx1^L148A/-* mice (Figure 1F, Suppl. Figure S2C), but increased short-term (ST) HSCs (LKS CD34+Flt3⁻)
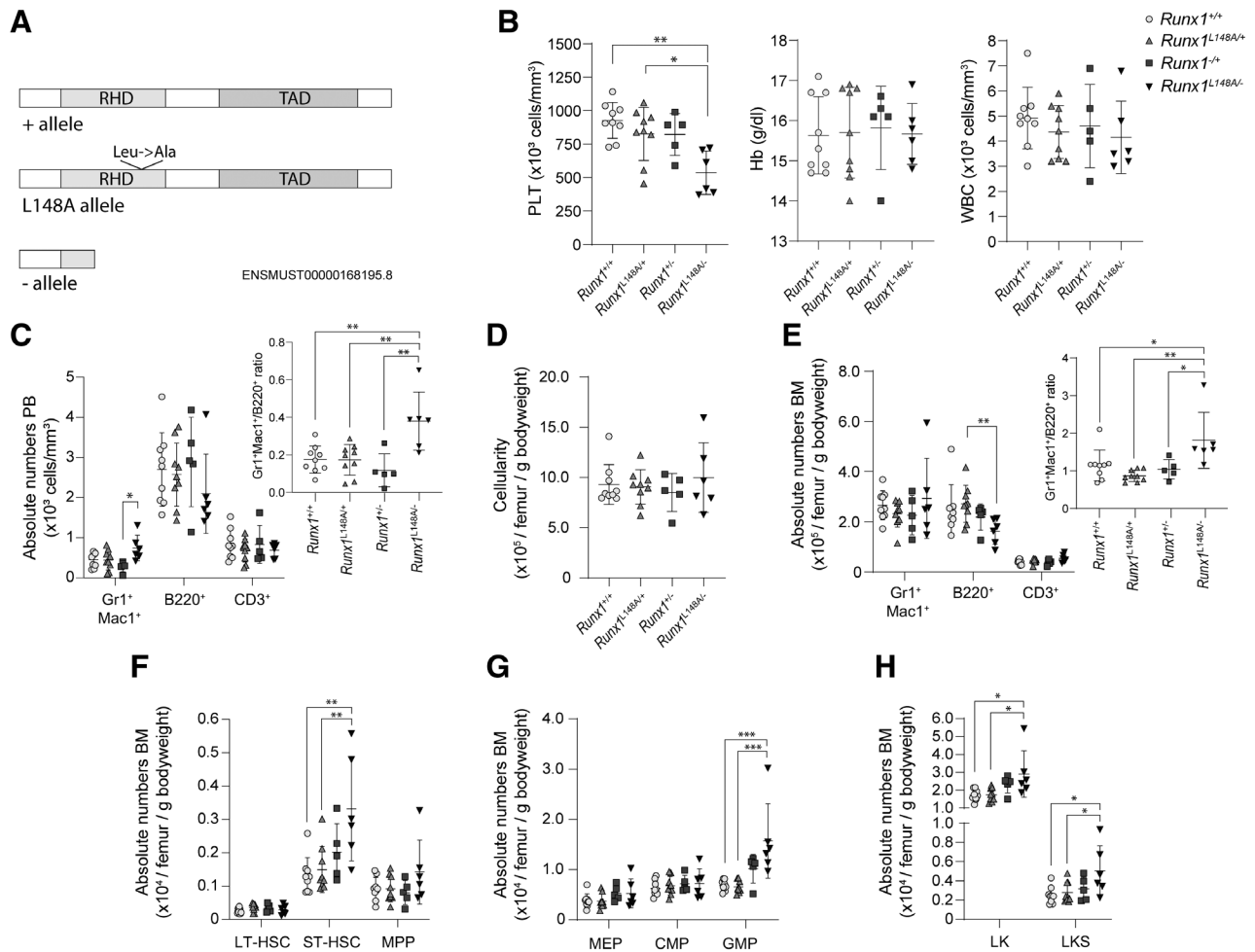
Figure 1. Germline loss-of-function of *Runx1* results in thrombocytopenia and a myeloid-biased hematopoiesis in *Runx1*^L148A/– mice. (A) Schematic representation of the RUNX1 protein showing the Runt homology domain (RHD) and Transactivation domain (TAD) and the consequences of mutant alleles on protein structure, shown is isoform b. (B) Peripheral blood values indicate the robust presence of thrombocytopenia in *Runx1*^L148A/– mice. (C) The number of white blood cell subsets indicates an increased myeloid/lymphoid ratio in *Runx1*^L148A/– mice. (D) Bone marrow cellularity. (E) Reduced numbers of bone marrow B220^+ B cells and an increased myeloid/lymphoid ratio in *Runx1*^L148A/– mice. (F) Increased numbers of LK and LKS subsets in *Runx1*^L148A/– mice. (G, H) Increased numbers of immunophenotypic granulocyte-monocyte progenitor (GMP) and short-term hematopoietic stem cells (LKS CD34^+Flt3^–) in *Runx1*^L148A/– mice. n = 9 *Runx1*^+/+, n = 9 *Runx1*^L148A/+, n = 5 *Runx1*^+/–, n = 6 *Runx1*^L148A/–. Data are indicated as mean ± SD; *$P < 0.05$, **$P < 0.01$, ***$P < 0.001$; significance tested with 2-tailed one-way ANOVA and Tukey-Kramer HSD post-hoc test. PLT = platelet; Hb = hemoglobin; WBC = white blood cell count; PB = peripheral blood; BM = bone marrow; LK = lin–cKit+Sca1-; LKS = lin–cKit+Sca1+; MEP = megakaryocyte-erythrocyte progenitor; CMP = common myeloid progenitor; GMP = granulocyte-monocyte progenitor; LT = long term; ST = short term; HSC = hematopoietic stem cell; MPP = multipotent progenitor.

and granulocyte-monocyte progenitor cells (GMPs, lin–cKit+Sca1- (LK) CD16/CD32+CD34+) were observed (Figure 1F-H; Suppl. Figure S2C). Of note, ST-HSCs defined by CD34+Flt3– expression constitute a rather heterogeneous population that likely also contains early myeloid-committed progenitor cells.[51]

Runx1^+/– mice did not show significant differences in any of these phenotypes, although a trend towards increased ST-HSCs and GMPs was observed (Figure 1B-H).

To examine the functional capacity of *Runx1*^L148A/– HSCs, we performed competitive transplant studies (Figure 2A) testing the LT reconstitution ability of *Runx1*^L148A/– HSCs versus wild-type HSCs. Mice were sacrificed 16 weeks after transplantation and donor contribution to reconstituted hematopoiesis was assessed. *Runx1*^L148A/– HSCs displayed reduced repopulation ability, as demonstrated by reduced CD45.2 chimerism in the peripheral blood (71.4% ± 5.5% vs 39.5% ± 14.4% for *Runx1*^+/+ and *Runx1*^L148A/– CD45.2 test cells, respectively). Within lymphocyte populations, however, impaired repopulation ability was only significant for the repopulation of lymphoid fractions (B220+ B cells 76.2% ± 7.6% vs 38.0 ± 9.8%; CD3e+ T cells 60.1% ± 6.9% vs 11.3% ± 6.4%, in the blood of transplanted animals; Figure 2B).

This was mirrored by a significantly and specifically reduced contribution of *Runx1*^L148A/– cells to B cells in the bone marrow (Figure 2C). The apparent discrepancy between *Runx1*^L148A/– contribution to T-cell reconstitution in the bone marrow and blood may be contributed to impaired extramedullary T-cell development defects associated with *Runx1* deficiency.[52]

Taken together, the data indicate that the combination of a null and hypomorphic *Runx1* allele results in robust thrombocytopenia and myeloid-biased hematopoiesis, in part because of an HSC intrinsic defect in lymphoid reconstitution ability. Malignant transformation, including the development of AML, was not observed in any of the *Runx1*^L148A/– mice examined by general assessment of their health status, organ inspection, peripheral blood and bone marrow cell counts, and immunophenotypic analyses of peripheral blood, bone marrow, and spleen, despite considerable follow-up of up to 8 months.

Targeted deletion of *Runx1* from bone marrow stromal cells

The contribution of *Runx1*-deficient non-hematopoietic cells to the hematopoietic phenotype of *RUNX1*-FPD patients is
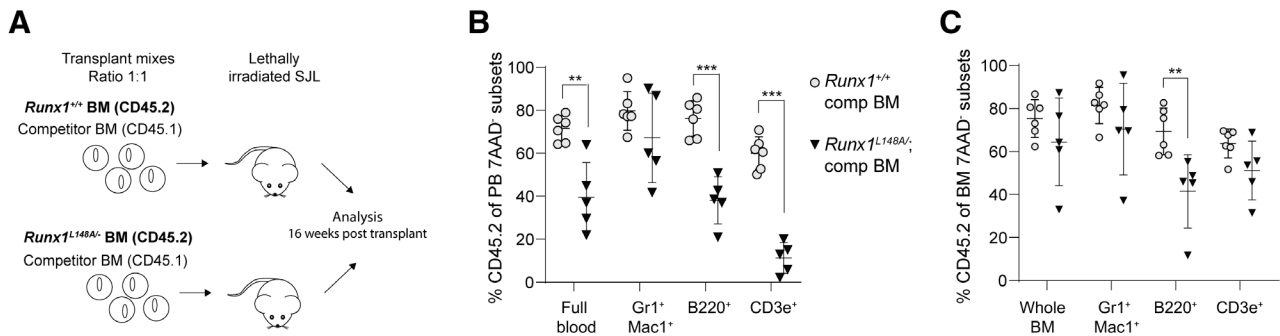
Figure 2. *Runx1*[L148A/−] HSCs have a competitive disadvantage in lymphoid reconstitution. (A) *Runx1*^{+/+} or *Runx1*[L148A/−] CD45.2 BM cells were competitively transplanted in a 1:1 ratio with CD45.1 competitor BM cells into lethally irradiated SJL mice that were sacrificed after 16 weeks. (B-C) *Runx1*[L148A/−] have a significant competitive disadvantage in the reconstitution of B220+ B lymphocytes as depicted by reduced chimerism in the blood (B) and bone marrow (C). n = 6 *Runx1*^{+/+}, n = 5 *Runx1*[L148A/+], data are indicated as mean ± SD; **$P < 0.01$, ***$P < 0.001$; significance tested with 2-tailed Student's t-test. BM = bone marrow; PB = peripheral blood.

incompletely understood. In particular, the potential contributions of bone marrow stromal cells (BMSCs), which constitute important HSC niches[20] and have been shown to potentially drive hematopoietic disruption and malignant transformation upon primary genetic alteration,[22–25] have not been rigorously assessed. To address this, we exploited a mouse model of targeted *Runx1* deletion from BMSCs expressing a Cre recombinase under the control of the mesenchyme-specific *Prrx1* promoter.[32,33,53,54] PRRX1 is involved in limb bud formation[33] and expressed in BMSCs throughout development.[37,55] Previous descriptions of the *Prrx1-cre* model (also known as *Prx1-cre*) confirmed robust targeting of approximately 90% of LepR expressing BMSCs that form a major source of factors supporting hematopoiesis.[54]

We crossed *Prrx1-cre* mice with mice in which the fifth exon of *Runx1* (previously annotated as exon 4) is flanked by *LoxP* sites (Figure 3A),[11,17] resulting in *Prrx1-cre;Runx1*^{fl/fl} mice that have previously been reported to have no obvious limb phenotype.[32]

Runx1 deletion from BMSCs and their progeny in this model was confirmed by genomic PCR, confirming recombination of *Runx1* in bone/bone marrow-containing tissues (collagenased bone fractions and toe) (Figure 3B), in line with the development of bone-associated cell types from PRRX1+ stromal cells (Figure 3B). The deletion was not observed in peripheral blood cells or the liver, confirming deletion specificity in tissues containing BMSCs and their differentiated progeny.

RNA sequencing of highly FACS purified CD51+Sca1+ (constituting an MSC-enriched fraction) and CD51+Sca1− (enriched for LepR+ osteo/adipolineage progenitor cells; OLC) confirmed expression of *Runx1* and *Prrx1* in these BMSC populations (Figure 3C, D) with specific excision of exon 5 in *Prrx1-cre;Runx1*^{fl/fl} animals (not introducing a frameshift) as demonstrated by DEXSeq analysis (Figure 3E).[47]

Recombination efficacy of the *Prrx1-cre* system was confirmed through analyses of collagenased bone fractions of *Prrx1-cre;TdTomato* mice (n = 3), demonstrating a high recombination efficiency in both MSC and OLC populations (with averages of 91.8% ± 2.0% and 87.7 ± 6.9%, respectively; Suppl. Figure S3A), very much in accordance with our RNA sequencing analysis using DEXSeq. Taken together, the data confirm very high recombination efficacy of stromal HSPC niches by the *Prrx1-cre* system in adult mice.

Deletion of *Runx1* from BMSCs did not alter their relative frequency within the bone marrow (Figure 3C) and had a relatively modest impact on the transcriptional wiring of BMSC fractions, with a limited number of genes significantly ($P < 0.05$) differentially expressed in MSCs (41 genes) and OLCs (170 genes) (Suppl. Figure S4A and Suppl. Table S1-2). Analysis of differentially expressed gene programs by GSEA revealed enrichment of

transcriptional programs indicative of inflammatory activation of BMSCs (Suppl. Figure S4B). Gene sets upregulated in both MSCs and OLCs included TNFα signaling via NF-κB and interferon signaling related programs, perhaps related to a previously documented role of RUNX1 in the dampening of inflammatory signaling via NF-κB[29–31] and interferon[57] signaling. Expression of genes implicated in HSC maintenance and regulation such as *Cxcl12* and *Kitl* (also known as *Scf*) were not differentially expressed in *Prrx1-cre;Runx1*^{fl/fl} BMSCs (Figure 3D).

The establishment of a mouse model with *Runx1* deficiency in BMSCs allowed us to interrogate the effects of *Runx1* deficiency in the mesenchymal niche on steady-state hematopoiesis. Blood and bone marrow analyses at the age of 42–46 weeks did not reveal any apparent hematopoietic phenotype. Sequential automated blood counts revealed no differences in either platelet count, hemoglobin, or white blood cell count (Figure 4A); neither were any white blood cell subsets altered in *Prrx1-cre;Runx1*^{fl/fl} mice, as assessed by flow cytometry of peripheral blood MNCs (Figure 4B). Analysis of the bone marrow revealed no difference in cellularity (Figure 4C). Bone marrow composition analysis using flow cytometry showed unaltered frequencies of white blood cell subsets (Figure 4D) and HSPC subsets (LK and LKS populations [Figure 4E], myeloid progenitors [Figure 4F], and early progenitors [Figure 4G]). Together, these data indicate that depletion of *Runx1* specifically from BMSCs does not result in alterations of steady-state hematopoiesis.

The *Runx1* deficient (micro) environment does not contribute to thrombocytopenia or myeloid-biased hematopoiesis in *Runx1*[L148A/−] mice

In the *Prrx1-cre;Runx1*^{fl/fl} model, we interrogated the contribution of *Runx1* deficiency, specifically in BMSCs, to steady-state hematopoiesis. It is, however, conceivable that other non-hematopoietic elements (including other components of the bone marrow microenvironment) contribute to the disruption of hematopoiesis in *RUNX1*-FPD. To investigate if *Runx1* deficiency in any other niche constituent could contribute to the hematopoietic phenotype of *Runx1*[L148A/−] mice, we transplanted wild-type hematopoietic cells into *Runx1*[L148A/−] and *Runx1*^{+/+} mice (Figure 5A). Two transplanted animals in the *Runx1*[L148A/−] group died after irradiation (8.5 Gy) and transplantation due to graft failure and infection respectively, precluding LT follow up of these mice. In the remaining transplant recipients near complete donor (CD45.1 wild type) chimerism was confirmed (Figure 5B) and mice followed up until 300 days after transplantation. Sequential automated peripheral blood counts did not show any differences in platelets, white blood cells, or hemoglobin (Figure 5C). No significant and consistent differences were found in the numbers of Gr1+Mac1+ granulocytes and
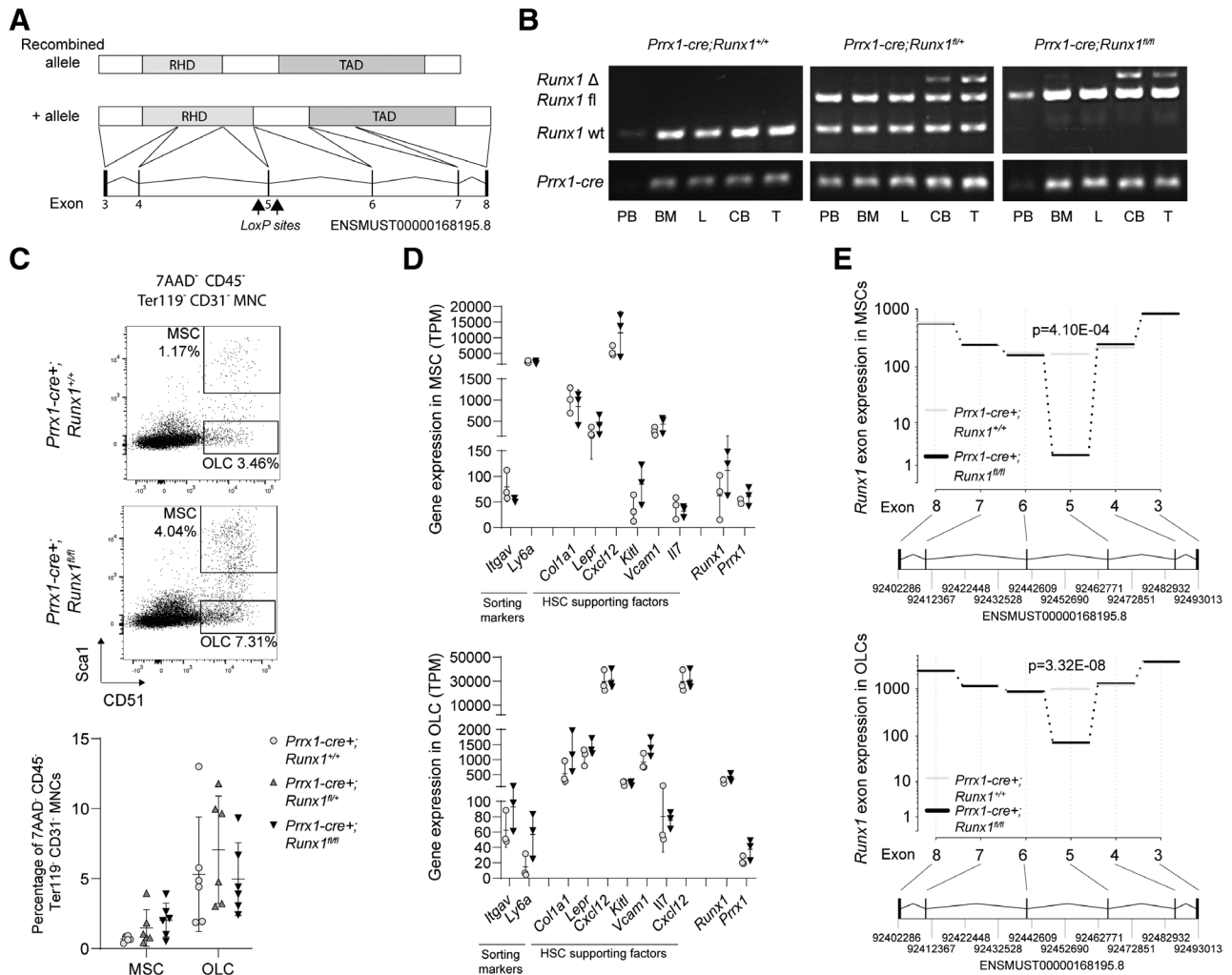
Figure 3. Targeted deletion of *Runx1* from bone marrow stromal cells in *Prrx1-cre;Runx1^{fl/fl}* mice. (A) Schematic diagram showing *LoxP* sites surrounding exon 5 of the *Runx1* gene and effect of recombination on the protein, shown is isoform b. (B) Genotyping by PCR confirms deletion of *Runx1* in bone-containing tissue (collagenased bone/bone marrow and toe) specifically, with a minor deletion band in bone marrow, reflecting low frequencies of BMSCs. (C) Representative FACS gating of BMSC populations (upper panel) and preservation of BMSC frequencies in *Prrx1-cre;Runx1^{fl/fl}* mice (lower panel). (D) Significant loss of *Runx1* exon 5 expression in both mesenchymal stem cell (MSC)- enriched and osteo/adipolineage progenitor cell-enriched (OLC) BMSC fractions from *Prrx1-cre;Runx1^{fl/fl}* mice. (E) No difference in gene expression of sorting markers and HSC supporting factors within MSC and OLC populations from *Prrx1-cre;Runx1^{fl/fl}* and control mice. n = 2/3 *Prrx1-cre;Runx1^{+/+}*, n = 3 *Prrx1-cre;Runx1^{fl/fl}*. RHD = Runt homology domain; TAD = transactivation domain; PB = peripheral blood; BM = bone marrow; L = liver; CB = collagenased bone/bone marrow; T = toe; MSC = mesenchymal stem cell-enriched BMSCs; OLC = osteo/adipolineage progenitor cell-enriched BMSCs.

B220$^+$ B cells in the peripheral blood (Figure 5D). Analysis of bone marrow revealed unaltered cellularity (Figure 5E) without significant differences in numbers of white blood cell subsets (Figure 5F), GMP, or ST-HSC numbers (Figure 5G–I).

Frequencies of MSC and OLC subsets within the bone marrow niche were unaltered in *Runx1^{L148A/−}* mice 10 months after transplantation (Suppl. Figure S5).

Conversely, when CD45.2 *Runx1^{L148A/−}* vs *Runx1^{+/+}* hematopoietic cells from 8-month-old mice were transplanted into lethally irradiated CD45.1 recipient mice, we observed that *Runx1^{L148A/−}* hematopoietic cells recapitulated the key hematopoietic features of *Runx1^{L148A/−}* germline mice, notably thrombocytopenia, myeloid/lymphoid skewing and an increase of ST-HSCs and GMPs (non-significantly) in the bone marrow (Suppl. Figure S6). Bone marrow CD45.2 chimerism was modestly lower (88.95% ± 6.57% SD vs 97.38% ± 1.13% SD, P = 0.003) for mice transplanted with *Runx1^{L148A/−}* cells, consistent with the observed reduced repopulation ability in competitive assays.

Collectively, the data from mice with targeted deletion of *Runx1* from BMSCs and the transplant in-out experiments with

Runx1^{L148A/−} mice argue against a significant contribution of the *RUNX1* deficient bone marrow microenvironment or ancillary, non-hematopoietic, cells to the hematopoietic phenotype of *Runx1^{L148A/−}* mice.

DISCUSSION

The cellular and molecular drivers of the hematopoietic defects in *RUNX1*-FPD are incompletely understood, in part because of the lack of disease models faithfully recapitulating the dominant-negative effects of *RUNX1* mutations in all cells of the organism. The lack of such models has also precluded formal insights into the potential contributions of ancillary, non-hematopoietic cells to the hematopoietic manifestations of this disease.

As complete loss of *Runx1* in mice confers embryonic lethality,[8,9] insights in disease biology have so far been obtained from observations in *Runx1^{+/−}* heterozygous mice (carrying the mutations in all cells but not recapitulating the dominant-negative effect that *RUNX1* mutations can have in a subset of patients)[4–7]
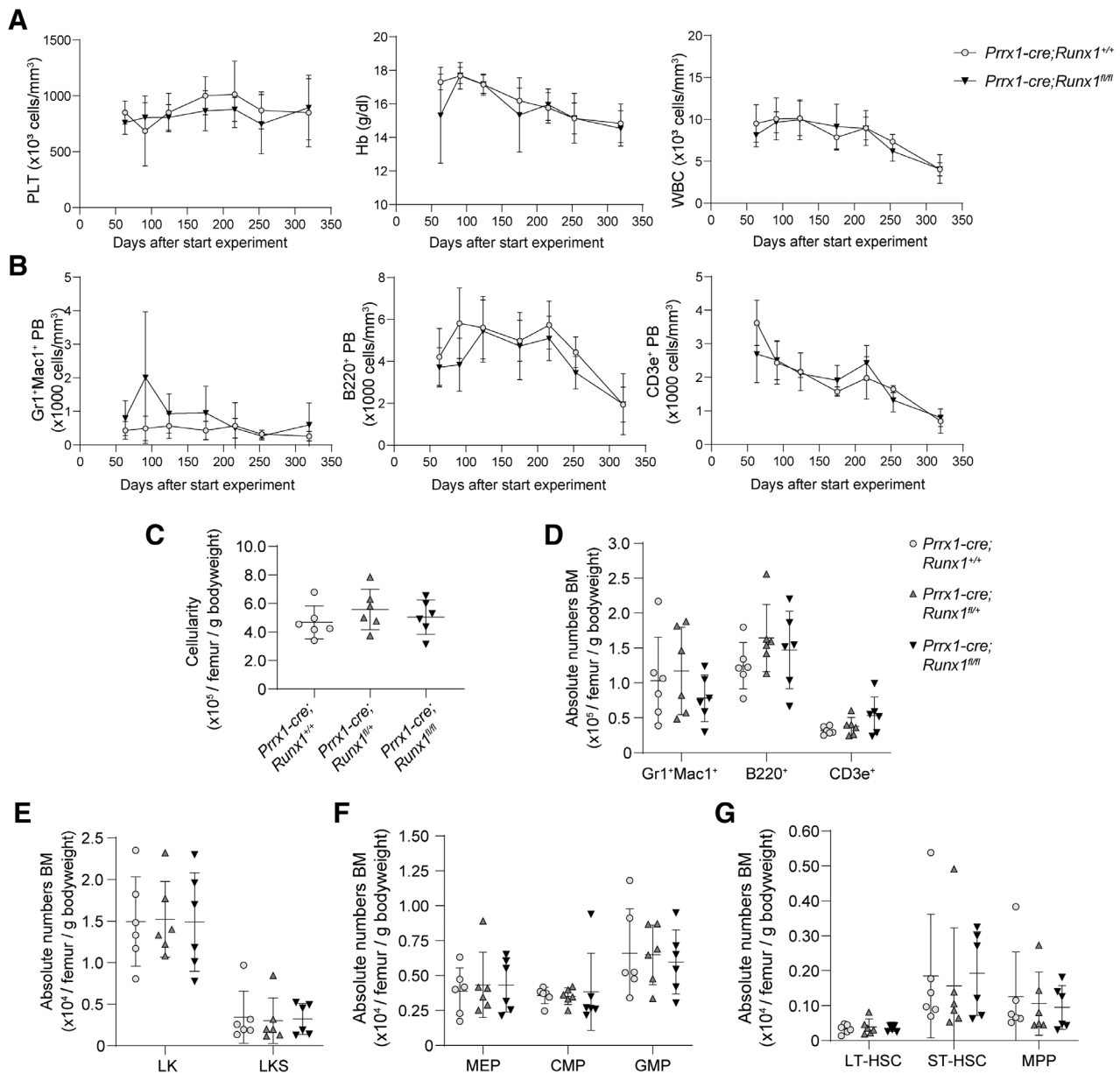
Figure 4. Targeted deletion of *Runx1* from bone marrow stromal cells does not disrupt hematopoiesis. Mice were examined at the age of 300–325 days. (A) Automated blood counts. (B) Numbers of Gr1+Mac1+ myeloid cells, B220+ B cells, and CD3e+ T cells in peripheral blood (PB). (C) Bone marrow (BM) cellularity. (D–G) Numbers of Gr1+Mac1+ myeloid cells, B220+ B cells, and CD3e+ T cells and HSPC subsets in the bone marrow. n = 6 *Prrx1-cre;Runx1+/+*, n = 6 *Prrx1-cre;Runx1fl/+*, n = 6 *Prrx1-cre;Runx1fl/fl*. Data are indicated as mean ± SD; significance tested with 2-tailed one-way ANOVA and Tukey-Kramer HSD post-hoc test. PLT = platelet; Hb = hemoglobin; WBC = white blood cell count; PB = peripheral blood; BM = bone marrow; LK = lin−cKit+Sca1-; LKS = lin−cKit+Sca1+; MEP = megakaryocyte-erythrocyte progenitor; CMP = common myeloid progenitor; GMP = granulocyte-monocyte progenitor; LT = long term; ST = short term; HSC = hematopoietic stem cell; MPP = multipotent progenitor.

or models in which the *Runx1* mutation was confined to hematopoietic cells (not recapitulating the omnipresence of the mutation in *RUNX1*-FPD patients).

Here, we report on the LT follow-up of mice harboring a hypomorphic germline mutation on a null background to model residual RUNX1 function below 50% as a proxy for dominant-negative mutations in *RUNX1*-FPD. The model recapitulates the thrombocytopenia found in patients and reveals an increase in myelopoiesis relative to lymphopoiesis, a finding that may carry relevance for the propensity for myeloid neoplasms in patients.

Our findings on the hematopoietic abnormalities of *Runx1L148A/−* mice seem largely in line with those reported in studies exploiting *Runx1* heterozygous mice[19,32] and those with

a targeted knockout of *Runx1* from hematopoietic cells,[10–17] converging on the notion that *Runx1* deficiency in hematopoietic cells results in a decrease in platelets, a defect in lymphoid cell production, and an increase in myeloid potential.

Thrombocytopenia has been a robust finding in conditional *Runx1* knockout mice, with multiple reports finding a marked decrease in bone marrow megakaryocytes and polyploidization defects.[10–12] Impaired lymphopoiesis, reflected in reduced B-cell numbers in bone marrow and blood and reduced T cells in the thymus have earlier been reported in conditional *Runx1* knockout mice.[11,12,15] Similarly, increased immunophenotypic GMPs[11,14] and increased myeloid colony forming capacity (in vitro)[10,11,19] seem reproducible hematopoietic phenotypes in mice, with potential relevance for human disease (iPSC models)
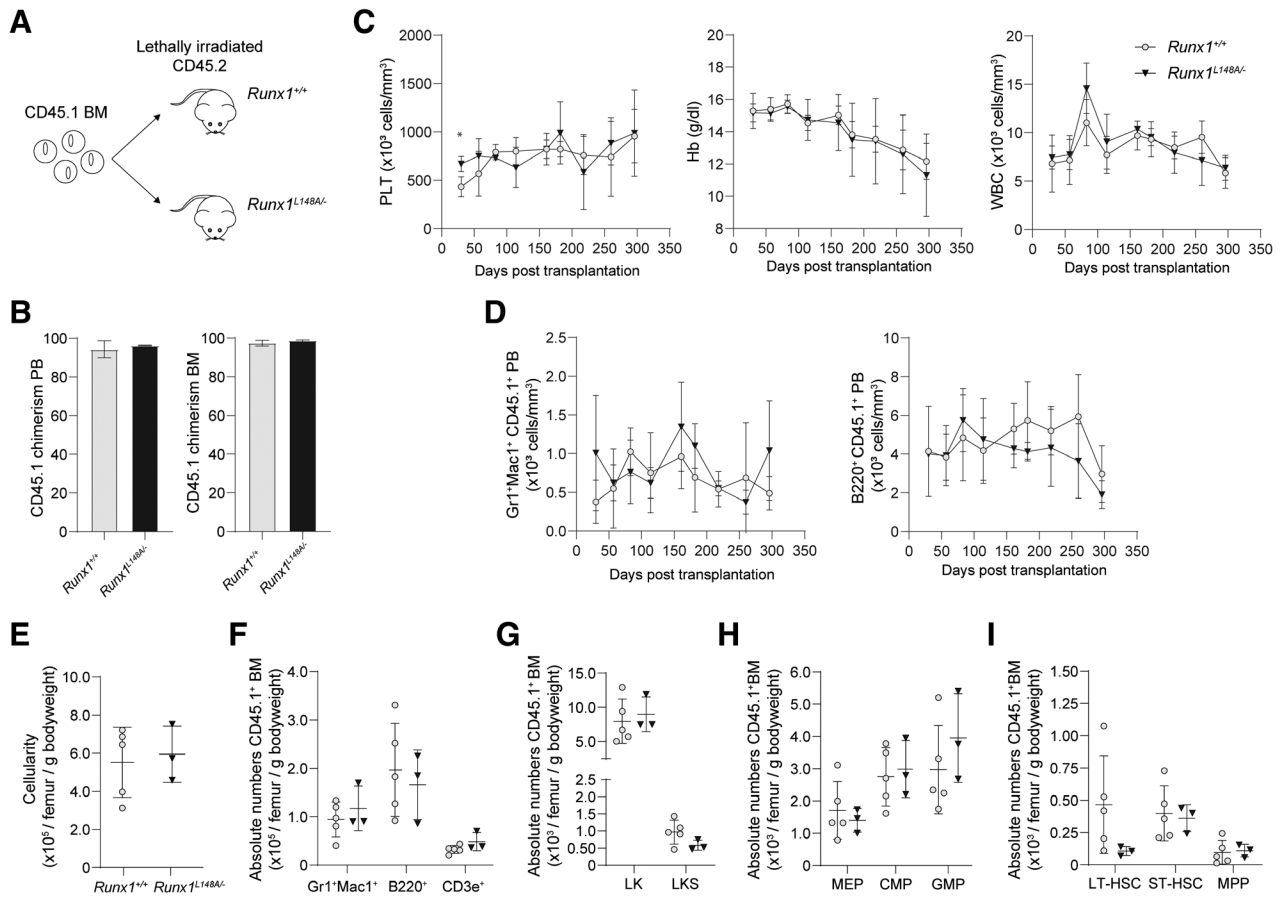
Figure 5. The *Runx1* deficient (micro) environment does not contribute to thrombocytopenia or myeloid-biased hematopoiesis in *Runx1*[L148A/–] mice. (A) *Runx1*^{+/+} and *Runx1*[L148A/–] mice were transplanted with CD45.1 bone marrow hematopoietic cells after lethal irradiation, and hematopoiesis was analyzed after 10 months. (B) Blood and bone marrow contained >90% donor cells in all mice. (C) Automated blood counts. (D) Numbers of donor-derived Gr1+Mac1+ myeloid cells and B220+ B cells in peripheral blood. (E–I) Numbers of donor-derived Gr1+Mac1+ myeloid cells, B220+ B cells, and CD3e+ T cells and HSPC subsets in the bone marrow. n = 5 *Runx1*^{+/+}, n = 3 *Runx1*[L148/–]. Data are indicated as mean ± SD; significance tested with 2-tailed Student's t-test, *$P <$ 0.05. BM = bone marrow; PLT = platelet; Hb = hemoglobin; WBC = white blood cell count; PB = peripheral blood; LK = lin−cKit+Sca1−; LKS = lin−cKit+Sca1+; MEP = megakaryocyte-erythrocyte progenitor; CMP = common myeloid progenitor; GMP = granulocyte-monocyte progenitor; LT = long term; ST = short term; HSC = hematopoietic stem cell; MPP = multipotent progenitor.

in which increased CFU-GM colony formation has also been observed.[6,58] The latter observation was present in an iPSC cell line from a patient with a dominant-negative mutation (*Runx1* R174Q),[4,5] and present in 1 of 2 tested iPSC cell lines from patients with a loss-of-function mutation (monoallelic *Runx1* deletion and *Runx1* R139X).[6,58] Although insufficient data is available to draw conclusions on genotype-phenotype relationships in *RUNX1*-FPD, the increase in the primitive myeloid compartment found in multiple experiments seems to be better reflected by *Runx1*[L148A/–] compared to *Runx1*^{+/–} mice.

The effects of *Runx1* deficiency on stem cell function, in particular their competitive repopulation ability, is relevant in the context of potential future gene correction and transplantation strategies, that are unlikely to be effective if residual, non-corrected *Runx1* deficient HSCs have a competitive advantage over corrected cells. Previous mouse models have led to conflicting conclusions, with increased repopulation ability reported in a heterozygous loss-of-function model,[19] while studies using *Mx1-cre;Runx1*^{fl/fl} bone marrow in transplantation setting reported failure to repopulate the lymphoid lineage.[10,11] Our finding that *Runx1*[L148A/–] HSCs have a competitive disadvantage to the repopulation ability of wild-type HSCs, in particular a significantly reduced contribution to the lymphoid lineage, is in line with the latter publications on *Runx1* null bone marrow.[10,11] Gene dosage-dependent effects of *Runx1* deficiency on stem cell

function may provide an explanation for reported differences, where heterozygous loss-of-function (represented by *Runx1*^{+/–} mice) may result in increased repopulation ability, whereas further reduction of RUNX1 function (as would be the case with dominant-negative mutations and represented by *Runx1*^{–/–} and *Runx1*[L148A/–] models) may deteriorate the competitive ability of HSCs to repopulate the marrow.

The establishment of *Runx1*[L148A/–] mice further allowed us to experimentally define the contribution of non-hematopoietic *Runx1* deficient cells on the hematopoietic manifestations. The bone marrow microenvironment, and particularly BMSCs, is pivotal in HSC maintenance and regulation, including roles in balancing myeloid versus lymphoid hematopoiesis,[21] and has been implicated in malignant transformation.[22–24] Transplantation of wild-type hematopoietic cells into the *Runx1* deficient environment did not recapitulate the hematopoietic phenotype of *Runx1*[L148A/–] mice, while transplanting *Runx1*[L148A/–] hematopoietic cells into a wild-type environment did, arguing against a driving contribution of ancillary cells to the thrombocytopenia and myeloid-biased hematopoiesis observed in these mice. This notion was corroborated in mice with targeted deletion of *Runx1* from BMSCs, the cellular components known to be critical determinants of HSC behavior and implicated in hematopoietic disruption and malignant transformation.[22–25] The experimental data arguing against a driving role of the bone

marrow microenvironment to thrombocytopenia seem in line with observations of hematopoietic recovery after allogeneic transplant in human patients, although detailed reports on LT hematopoietic recovery after transplant in *RUNX1*-FPD seem rather scarce.[59–61]

Collectively, previous reports recapitulating hematopoietic defects by hematopoietic cell-specific deletion of *Runx1*[10–17] and our current studies do not support a driving role of the (bone marrow) microenvironment to disease pathogenesis. We can, however, not exclude the formal possibility that *Runx1* deficient hematopoietic cells cooperate with a *Runx1* deficient environment at some point during malignant transformation. For example, it may be hypothesized that inflammatory exogenous stimuli, not recapitulated in our mouse model, such as repeated infection, aging, the microbiome,[62] and/or the acquisition of additional mutations may lead to further inflammatory activation of *Runx1* deficient stromal and hematopoietic cells that may be unable to dampen this inflammatory signaling. Such exaggerated inflammatory activation of stromal cells may subsequently promote genotoxic stress in HSPC and promote the selection of mutated clones resistant to inflammatory signaling.[25,63–66]

Future experiments will have to shed further light on these possibilities. Our characterization of the *Runx1*[L148A/–] and *Prrx1-cre;Runx1*^{fl/fl} models is anticipated to foster these studies and facilitate other studies aimed at further elucidating the pathogenic mechanisms underlying *RUNX1*-FPD.

AUTHOR CONTRIBUTIONS

MHGPR conceptualized the project and acquired funding. NAS provided resources and scientific input. MPTE and MHGPR designed experiments. MPTE, EP, CVD, PMHVS, TVDVT, and EMJB performed experimental procedures. MPTE, EP, MJWW, and MAS curated and analyzed data. MPTE, EP, and MJWW provided data visualization. MPTE, EP, and MHGPR wrote the article. MHGPR supervised the project.

REFERENCES

1. Brown AL, Arts P, Carmichael CL, et al. RUNX1-mutated families show phenotype heterogeneity and a somatic mutation profile unique to germline predisposed AML. *Blood Adv*. 2020;4:1131–1144.
2. Bellissimo DC, Speck NA. RUNX1 Mutations in Inherited and Sporadic Leukemia. *Front Cell Dev Biol*. 2017;5:111.
3. Godley LA. Inherited predisposition to acute myeloid leukemia. *Semin Hematol*. 2014;51:306–321.
4. Michaud J, Wu F, Osato M, et al. In vitro analyses of known and novel RUNX1/AML1 mutations in dominant familial platelet disorder with predisposition to acute myelogenous leukemia: implications for mechanisms of pathogenesis. *Blood*. 2002;99:1364–1372.
5. Matheny CJ, Speck ME, Cushing PR, et al. Disease mutations in RUNX1 and RUNX2 create nonfunctional, dominant-negative, or hypomorphic alleles. *EMBO J*. 2007;26:1163–1175.
6. Antony-Debre I, Manchev VT, Balayn N, et al. Level of RUNX1 activity is critical for leukemic predisposition but not for thrombocytopenia. *Blood*. 2015;125:930–940.
7. Latger-Cannard V, Philippe C, Bouquet A, et al. Haematological spectrum and genotype-phenotype correlations in nine unrelated families with RUNX1 mutations from the French network on inherited platelet disorders. *Orphanet J Rare Dis*. 2016;11:49.
8. Okuda T, van Deursen J, Hiebert SW, et al. AML1, the target of multiple chromosomal translocations in human leukemia, is essential for normal fetal liver hematopoiesis. *Cell*. 1996;84:321–330.
9. Wang Q, Stacy T, Binder M, et al. Disruption of the Cbfa2 gene causes necrosis and hemorrhaging in the central nervous system and blocks definitive hematopoiesis. *Proc Natl Acad Sci USA*. 1996;93:3444–3449.
10. Ichikawa M, Asai T, Saito T, et al. AML-1 is required for megakaryocytic maturation and lymphocytic differentiation, but not for maintenance of hematopoietic stem cells in adult hematopoiesis. *Nat Med*. 2004;10:299–304.
11. Growney JD, Shigematsu H, Li Z, et al. Loss of Runx1 perturbs adult hematopoiesis and is associated with a myeloproliferative phenotype. *Blood*. 2005;106:494–504.
12. Putz G, Rosner A, Nuesslein I, et al. AML1 deletion in adult mice causes splenomegaly and lymphomas. *Oncogene*. 2006;25:929–939.
13. Motoda L, Osato M, Yamashita N, et al. Runx1 protects hematopoietic stem/progenitor cells from oncogenic insult. *Stem Cells*. 2007;25:2976–2986.
14. Ichikawa M, Goyama S, Asai T, et al. AML1/Runx1 negatively regulates quiescent hematopoietic stem cells in adult hematopoiesis. *J Immunol*. 2008;180:4402–4408.
15. Chen MJ, Yokomizo T, Zeigler BM, et al. Runx1 is required for the endothelial to haematopoietic cell transition but not thereafter. *Nature*. 2009;457:887–891.
16. Jacob B, Osato M, Yamashita N, et al. Stem cell exhaustion due to Runx1 deficiency is prevented by Evi5 activation in leukemogenesis. *Blood*. 2010;115:1610–1620.
17. Cai X, Gaudet JJ, Mangan JK, et al. Runx1 loss minimally impacts long-term hematopoietic stem cells. *PLoS One*. 2011;6:e28430e28430.
18. Cai X, Gao L, Teng L, et al. Runx1 deficiency decreases ribosome biogenesis and confers stress resistance to hematopoietic stem and progenitor cells. *Cell Stem Cell*. 2015;17:165–177.
19. Sun W, Downing JR. Haploinsufficiency of AML1 results in a decrease in the number of LTR-HSCs while simultaneously inducing an increase in more mature progenitors. *Blood*. 2004;104:3565–3572.
20. Morrison SJ, Scadden DT. The bone marrow niche for haematopoietic stem cells. *Nature*. 2014;505:327–334.
21. Mendez-Ferrer S, Bonnet D, Steensma DP, et al. Bone marrow niches in haematological malignancies. *Nat Rev Cancer*. 2020;20:285–298.
22. Raaijmakers MH, Mukherjee S, Guo S, et al. Bone progenitor dysfunction induces myelodysplasia and secondary leukaemia. *Nature*. 2010;464:852–857.
23. Kode A, Manavalan JS, Mosialou I, et al. Leukaemogenesis induced by an activating beta-catenin mutation in osteoblasts. *Nature*. 2014;506:240–244.
24. Dong L, Yu WM, Zheng H, et al. Leukaemogenic effects of Ptpn11 activating mutations in the stem cell microenvironment. *Nature*. 2016;539:304–308.
25. Zambetti NA, Ping Z, Chen S, et al. Mesenchymal inflammation drives genotoxic stress in hematopoietic stem cells and predicts disease evolution in human pre-leukemia. *Cell Stem Cell*. 2016;19:613–627.
26. Tang CY, Chen W, Luo Y, et al. Runx1 up-regulates chondrocyte to osteoblast lineage commitment and promotes bone formation by enhancing both chondrogenesis and osteogenesis. *Biochem J*. 2020;477:2421–2438.
27. Tang CY, Wu M, Zhao D, et al. Runx1 is a central regulator of osteogenesis for bone homeostasis by orchestrating BMP and WNT signaling pathways. *PLoS Genet*. 2021;17:e1009233.
28. Tang J, Xie J, Chen W, et al. Runt-related transcription factor 1 is required for murine osteoblast differentiation and bone formation. *J Biol Chem*. 2020;295:11669–11681.
29. Tang X, Sun L, Jin X, et al. Runt-related transcription factor 1 regulates LPS-induced acute lung injury via NF-kappaB signaling. *Am J Respir Cell Mol Biol*. 2017;57:174–183.
30. Nakagawa M, Shimabe M, Watanabe-Okochi N, et al. AML1/RUNX1 functions as a cytoplasmic attenuator of NF-kappaB signaling in the repression of myeloid tumors. *Blood*. 2011;118:6626–6637.
31. Bellissimo DC, Chen CH, Zhu Q, et al. Runx1 negatively regulates inflammatory cytokine production by neutrophils in response to Toll-like receptor signaling. *Blood Adv*. 2020;4:1145–1158.

32. Soung do Y, Talebian L, Matheny CJ, et al. Runx1 dose-dependently regulates endochondral ossification during skeletal development and fracture healing. *J Bone Miner Res*. 2012;27:1585–1597.

33. Logan M, Martin JF, Nagy A, et al. Expression of Cre Recombinase in the developing mouse limb bud driven by a Prxl enhancer. *Genesis*. 2002;33:77–80.

34. Madisen L, Zwingman TA, Sunkin SM, et al. A robust and high-throughput Cre reporting and characterization system for the whole mouse brain. *Nat Neurosci*. 2010;13:133–140.

35. Zambetti NA, Bindels EM, Van Strien PM, et al. Deficiency of the ribosome biogenesis gene Sbds in hematopoietic stem and progenitor cells causes neutropenia in mice by attenuating lineage progression in myelocytes. *Haematologica*. 2015;100:1285–1293.

36. Ping Z, Chen S, Hermans SJF, et al. Activation of NF-kappaB driven inflammatory programs in mesenchymal elements attenuates hematopoiesis in low-risk myelodysplastic syndromes. *Leukemia*. 2019;33:536–541.

37. Kenswil KJG, Pisterzi P, Sanchez-Duffhues G, et al. Endothelium-derived stromal cells contribute to hematopoietic bone marrow niche formation. *Cell Stem Cell*. 2021;28:653–670.e11.

38. Andrews S. FastQC: A Quality Control Tool for High Throughput Sequence Data. 2022. http://www.bioinformatics.babraham.ac.uk/projects/fastqc/. Accessed December 30, 2022.

39. Pertea G. gpertea/fqtrim: fqtrim release v0.9.7. 2022. https://zenodo.org/record/1185412#.YsabCRVByUk. Accessed January 9, 2023.

40. Patro R, Duggal G, Love MI, et al. Salmon provides fast and bias-aware quantification of transcript expression. *Nat Methods*. 2017;14:417–419.

41. Soneson C, Love MI, Robinson MD. Differential analyses for RNA-seq: transcript-level estimates improve gene-level inferences. *F1000Res*. 2015;4:1521.

42. Love MI, Huber W, Anders S. Moderated estimation of fold change and dispersion for RNA-seq data with DESeq2. *Genome Biol*. 2014;15:550.

43. Stephens M. False discovery rates: a new deal. *Biostatistics*. 2017;18:275–294.

44. Mootha VK, Lindgren CM, Eriksson KF, et al. PGC-1alpha-responsive genes involved in oxidative phosphorylation are coordinately downregulated in human diabetes. *Nat Genet*. 2003;34:267–273.

45. Subramanian A, Tamayo P, Mootha VK, et al. Gene set enrichment analysis: a knowledge-based approach for interpreting genome-wide expression profiles. *Proc Natl Acad Sci USA*. 2005;102:15545–15550.

46. Liberzon A, Subramanian A, Pinchback R, et al. Molecular signatures database (MSigDB) 3.0. *Bioinformatics*. 2011;27:1739–1740.

47. Anders S, Reyes A, Huber W. Detecting differential usage of exons from RNA-seq data. *Genome Res*. 2012;22:2008–2017.

48. Reyes A, Anders S, Weatheritt RJ, et al. Drift and conservation of differential exon usage across tissues in primate species. *Proc Natl Acad Sci USA*. 2013;110:15377–15382.

49. Forster A, Decker M, Schlegelberger B, et al. Beyond pathogenic RUNX1 germline variants: the spectrum of somatic alterations in RUNX1-familial platelet disorder with predisposition to hematologic malignancies. *Cancers (Basel)*. 2022;14:3431.

50. Li Z, Yan J, Matheny CJ, et al. Energetic contribution of residues in the Runx1 Runt domain to DNA binding. *J Biol Chem*. 2003;278:33088–33096.

51. Oguro H, Ding L, Morrison SJ. SLAM family markers resolve functionally distinct subpopulations of hematopoietic stem cells and multipotent progenitors. *Cell Stem Cell*. 2013;13:102–116.

52. Mevel R, Draper JE, Lie ALM, et al. RUNX transcription factors: orchestrators of development. *Development*. 2019;146:dev.148296.

53. Greenbaum A, Hsu YM, Day RB, et al. CXCL12 in early mesenchymal progenitors is required for haematopoietic stem-cell maintenance. *Nature*. 2013;495:227–230.

54. Yue R, Zhou BO, Shimada IS, et al. Leptin receptor promotes adipogenesis and reduces osteogenesis by regulating mesenchymal stromal cells in adult bone marrow. *Cell Stem Cell*. 2016;18:782–796.

55. Wolock SL, Krishnan I, Tenen DE, et al. Mapping distinct bone marrow niche populations and their differentiation paths. *Cell Rep*. 2019;28:302–311.e5.

56. Ding L, Saunders TL, Enikolopov G, et al. Endothelial and perivascular cells maintain haematopoietic stem cells. *Nature*. 2012;481:457–462.

57. Hu Y, Pan Q, Zhou K, et al. RUNX1 inhibits the antiviral immune response against influenza A virus through attenuating type I interferon signaling. *Virol J*. 2022;19:39.

58. Bluteau D, Gilles L, Hilpert M, et al. Down-regulation of the RUNX1-target gene NR4A3 contributes to hematopoiesis deregulation in familial platelet disorder/acute myelogenous leukemia. *Blood*. 2011;118:6310–6320.

59. Schmit JM, Turner DJ, Hromas RA, et al. Two novel RUNX1 mutations in a patient with congenital thrombocytopenia that evolved into a high grade myelodysplastic syndrome. *Leuk Res Rep*. 2015;4:24–27.

60. Buijs A, Poddighe P, van Wijk R, et al. A novel CBFA2 single-nucleotide mutation in familial platelet disorder with propensity to develop myeloid malignancies. *Blood*. 2001;98:2856–2858.

61. Owen CJ, Toze CL, Koochin A, et al. Five new pedigrees with inherited RUNX1 mutations causing familial platelet disorder with propensity to myeloid malignancy. *Blood*. 2008;112:4639–4645.

62. Vicente-Duenas C, Janssen S, Oldenburg M, et al. An intact gut microbiome protects genetically predisposed mice against leukemia. *Blood*. 2020;136:2003–2017.

63. Hormaechea-Agulla D, Matatall KA, Le DT, et al. Chronic infection drives Dnmt3a-loss-of-function clonal hematopoiesis via IFNgamma signaling. *Cell Stem Cell*. 2021;28:1428–1442.e6.

64. Muto T, Walker CS, Choi K, et al. Adaptive response to inflammation contributes to sustained myelopoiesis and confers a competitive advantage in myelodysplastic syndrome HSCs. *Nat Immunol*. 2020;21:535–545.

65. Avagyan S, Henninger JE, Mannherz WP, et al. Resistance to inflammation underlies enhanced fitness in clonal hematopoiesis. *Science*. 2021;374:768–772.

66. Pronk E, Raaijmakers M. The mesenchymal niche in MDS. *Blood*. 2019;133:1031–1038.